

Simple broadband signal detection at the fundamental limit

Anthony M. Polloreno¹ and Graeme Smith¹

¹Department of Applied Mathematics and Institute for Quantum Computing,
University of Waterloo, 200 University Avenue West, Waterloo, Ontario, N2L 3G1, Canada

(Dated: January 28, 2026)

Broadband detection of a weak oscillatory field with unknown carrier frequency underlies magnetometry, axion searches and gravitational-wave sensing. We show that the Grover-like integration-time lower bound for this task is a geometric corollary an upper bound on the integrated quantum Fisher information, a metrological constraint. We further give an all-analog multi-resonant protocol based on a randomized Su-Schrieffer-Heeger control Hamiltonian and an m -register GHZ probe and verify near-optimal scaling through simulation.

Quantum sensors convert weak classical fields into measurable changes of a quantum state. For oscillating signals, coherent control enables strong narrowband selectivity, but in many settings the carrier frequency is not known a priori and may lie anywhere within a wide band. The resulting bandwidth-sensitivity tradeoff is a recurring bottleneck in AC magnetometry, noise spectroscopy [1, 2] and proposed searches for axion-like dark matter and gravitational-wave detection [3, 4].

A recent line [5–13] of work on quantum-algorithmic sensing emphasizes that broadband detection resembles an unstructured search problem and derives a sensing-time lower bound by analogy with Grover’s algorithm [14, 15]. This raises a natural question: *is saturating the lower bound on broadband sensing inherently computational (requiring a quantum computer), or is it fundamentally metrological (achievable by coherent control and measurement alone)?* We argue here for the latter. We connect broadband detection directly to the integrated quantum Fisher information (IQFI) and show how the bound in Ref. [15] appears as an IQFI-based bandwidth constrain. We conclude by giving a concrete multi-resonant control construction based on a randomized SSH Hamiltonian that distributes sensitivity across a wide band and empirically attains the expected scaling.

Broadband AC detection problem We formalize broadband detection (as in Ref. [15]) as a promise problem $\text{AC}[B_{\min}, \Delta\omega]$: given an oscillatory field

$$B(t) = B \cos(\omega t + \varphi), \quad (1)$$

with unknown amplitude B , phase φ , and frequency $\omega \in \Delta\omega := [\omega_{\min}, \omega_{\max}]$, $|\Delta\omega| := \omega_{\max} - \omega_{\min}$, decide whether there exists a signal with $B \geq B_{\min}$ and $\omega \in \Delta\omega$ or if $B = 0$, in total interrogation time T . We consider the standard high-frequency regime, taking $\omega_{\min} \gtrsim B_{\min}$ to exclude the quasi-static limit (where DC protocols suffice, *cf* [15]). We focus on the genuinely broadband regime $|\Delta\omega| \gg B_{\min}$ (mB_{\min} when an m -register GHZ enhancement is used [16, 17]).

Integrated quantum Fisher information Our general setup can be seen in Figure 1. Let $\rho(B, \omega; T)$ be the quantum state of a probe system after evolving for time

T under a controlled, time-dependent Hamiltonian

$$H(t) = G(t) + B \cos(\omega t + \varphi) Z_{\text{tot}}, \quad Z_{\text{tot}} := \sum_{\ell=1}^m Z^{(\ell)}, \quad (2)$$

where $Z^{(\ell)}$ is the (known) single-register signal generator acting on register ℓ , and $G(t)$ is an arbitrary control Hamiltonian determined by the chosen sensing protocol. $J(B|\omega, T)$ is the quantum Fisher information (QFI) of $\rho(B, \omega; T)$ with respect to B after sensing time T and at a given frequency ω . The QFI captures the sensitivity of a protocol to a parameter B via the quantum Cramer Rao bound [18]. To quantify the total sensitivity of a protocol across a band, we use the IQFI [19–22]

$$K(B, T) := \int_{\Delta\omega} d\omega J(B|\omega, T). \quad (3)$$

Fundamentally any sensing protocol will consist of a time-dependent control Hamiltonian, but it is often helpful to conceptualize a protocol as a discrete sequence of unitaries. A key result of Ref. [20] is that for a discrete control protocol consisting of N unitary control operations over total time T , the IQFI is bounded as $K = O(NT)$. A continuous protocol can be approximated by piecewise-constant controls with step size δt , giving $N = T/\delta t$ and hence a leading contribution $O(T^2/\delta t)$. The leading discretization (Trotter) error adds a competing term that scales as $O(B^2 T^2 \delta t)$ (with additional protocol-dependent prefactors) [20]. Absorbing protocol-dependent constants into $C_1, C_2 > 0$ gives the generic bound

$$K(B, T; \delta t) \leq \frac{C_1 T^2}{\delta t} + C_2 B^2 T^2 \delta t, \quad (4)$$

with negligible higher-order terms in the regime of interest. Optimizing over δt yields

$$\delta t_* = \sqrt{\frac{C_1}{C_2}} \frac{1}{B}, \quad (5)$$

and therefore an overall (continuous-control) IQFI ceiling of the form

$$K(B, T) \leq C B T^2, \quad (6)$$

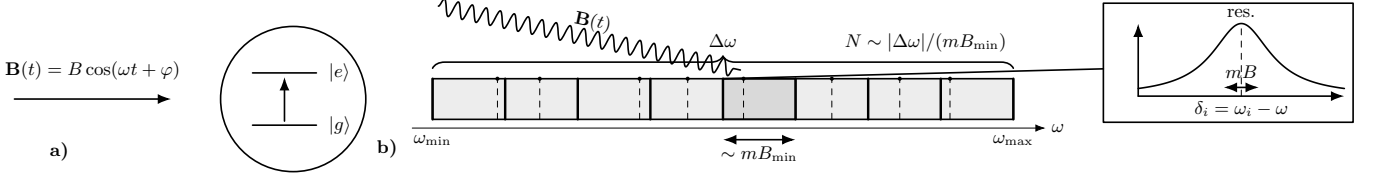


FIG. 1: Simple broadband sensing by internal band engineering. a) An incoming AC magnetic field field excites a transition from the ground state ($|g\rangle$) to an excited state ($|e\rangle$). b) Broadband sensing. Vertical dashed lines indicate engineered transition frequencies $\{\omega_i\}$ spanning $\Delta\omega$, approximating a grid of spacing $\sim mB_{\min}$ (solid lines). Each resonance contributes a broadened Rabi response of width $\sim mB$ (inset). A randomized construction may require a mild $\log r$ oversampling to avoid rare large gaps (see End Matter).

for a constant $C > 0$. This is saturated by the $\Theta(BT^2)$ scaling achievable via resonant Rabi dynamics [20].

IQFI as a discrimination statistic Ref. [20] shows that the IQFI cleanly separates perturbative and non-perturbative regimes. For perturbative fields ($BT \ll 1$), one has $K(B, T) = O(T)$, while in the nonperturbative regime $K(B, T)$ can grow quadratically in time as $K(B, T) = O(BT^2)$, saturating the fundamental bound in Eq. (6). As a result, as we show in detail below, broadband detection can be reduced to discriminating linear from quadratic IQFI growth. A simple statistical framework for performing this task is as follows. Fix $q > 1$ and choose a base time T with $B_{\min}T = \Theta(1)$ and run the sensing protocol for times T and qT .

Define the estimated log-log slope $\hat{\alpha} = (\log \hat{K}(B, qT) - \log \hat{K}(B, T)) / (\log q)$. Under null hypothesis H_0 (perturbative regime / effectively no signal) the mean slope is ≤ 1 , while under alternative hypothesis H_1 (nonperturbative regime) it approaches 2. A threshold at $3/2$ yields, for a constant $C > 0$, a probability of error bounded by $2 \exp(-CN_{\text{sh}} \log^2 q)$ via standard Hoeffding and Chernoff bounds [23, 24]. Thus $N_{\text{sh}} \gtrsim (1/\log^2 q) \log(1/\delta)$ shots at each time achieve error $\leq \delta$, i.e. $O(\log(1/\delta))$ total shots. A simple two-time hypothesis test is given in detail in the End Matter.

From distinguishability to an IQFI witness The QFI induces the Bures/Fubini-Study geometry of quantum states [25]. Fix (ω, T) and consider the one-parameter family

$$\rho_{B'} \equiv \rho(B'|\omega, T), \quad B' \in [0, B], \quad (7)$$

which traces out a curve on the state manifold. A convenient distinguishability statistic is the infidelity

$$p_{\text{det}}(B, \omega, T) := 1 - F(\rho_0, \rho_B), \quad (8)$$

where F is the Uhlmann fidelity [26]. For pure ρ_0 (as in our protocol), p_{det} is exactly the probability that a projective measurement onto the $B = 0$ state detects a deviation. More generally, any constant-bias discrimination implies $F(\rho_0, \rho_B) \leq 1 - \Omega(1)$ by the Fuchs-van de Graaf inequalities [27], so bounding p_{det} suffices to bound the fidelity up to constants.

Define the Bures angle [28, 29]

$$\theta_\omega(B, T) = \arcsin \sqrt{p_{\text{det}}(B, \omega, T)} = \arccos \sqrt{F(\rho_0, \rho_B)}. \quad (9)$$

Along the curve the QFI supplies the line element $ds = \frac{1}{2} \sqrt{J(B'|\omega, T)} dB'$, hence the curve length is

$$\ell(B|\omega, T) = \frac{1}{2} \int_0^B dB' \sqrt{J(B'|\omega, T)}. \quad (10)$$

Since the Bures angle gives the geodesic distance [25, 30, 31] and the geodesic distance is no larger than path length, $\theta_\omega(B, T) \leq \ell(B|\omega, T)$, and by Cauchy-Schwarz,

$$\frac{1}{B} \int_0^B dB' J(B'|\omega, T) \geq \frac{4}{B^2} \theta_\omega(B, T)^2. \quad (11)$$

Integrating over ω motivates the finite-displacement witness $K^{\text{FD}}(B, T) := \frac{4}{B^2} \int_{\Delta\omega} d\omega \theta_\omega(B, T)^2$. Using the IQFI ceiling in Eq. (6) for each $B' \in [0, B]$ gives

$$K^{\text{FD}}(B, T) \leq \frac{C}{2} B T^2. \quad (12)$$

Now suppose there is a broadband detection protocol such that there exists $p_0 > 0$ such that $p_{\text{det}}(B_{\min}, \omega, T) \geq p_0$, for all $\omega \in \Delta\omega$. Then $\theta_\omega(B_{\min}, T) \geq \theta_0 := \arcsin \sqrt{p_0}$ for all ω , so

$$K^{\text{FD}}(B_{\min}, T) \geq \frac{4\theta_0^2}{B_{\min}^2} |\Delta\omega|. \quad (13)$$

Combining (12) and (13) yields the scaling

$$T \gtrsim \frac{\sqrt{|\Delta\omega|}}{B_{\min}^{3/2}}. \quad (14)$$

This recovers the main result of Ref. [15] as a geometric corollary of the IQFI ceiling (6). With an m -register GHZ probe, the relevant Rabi scale is mB_{\min} , giving $T \gtrsim \sqrt{|\Delta\omega| / (mB_{\min})^{3/2}}$.

Single-frequency inference via spectral flatness In a sensing instance there is a fixed unknown ω^* . To relate single-frequency data to a band-integrated witness, we certify offline that the response has no deep spectral holes. Define the displacement-density $s_\omega(B, T) :=$

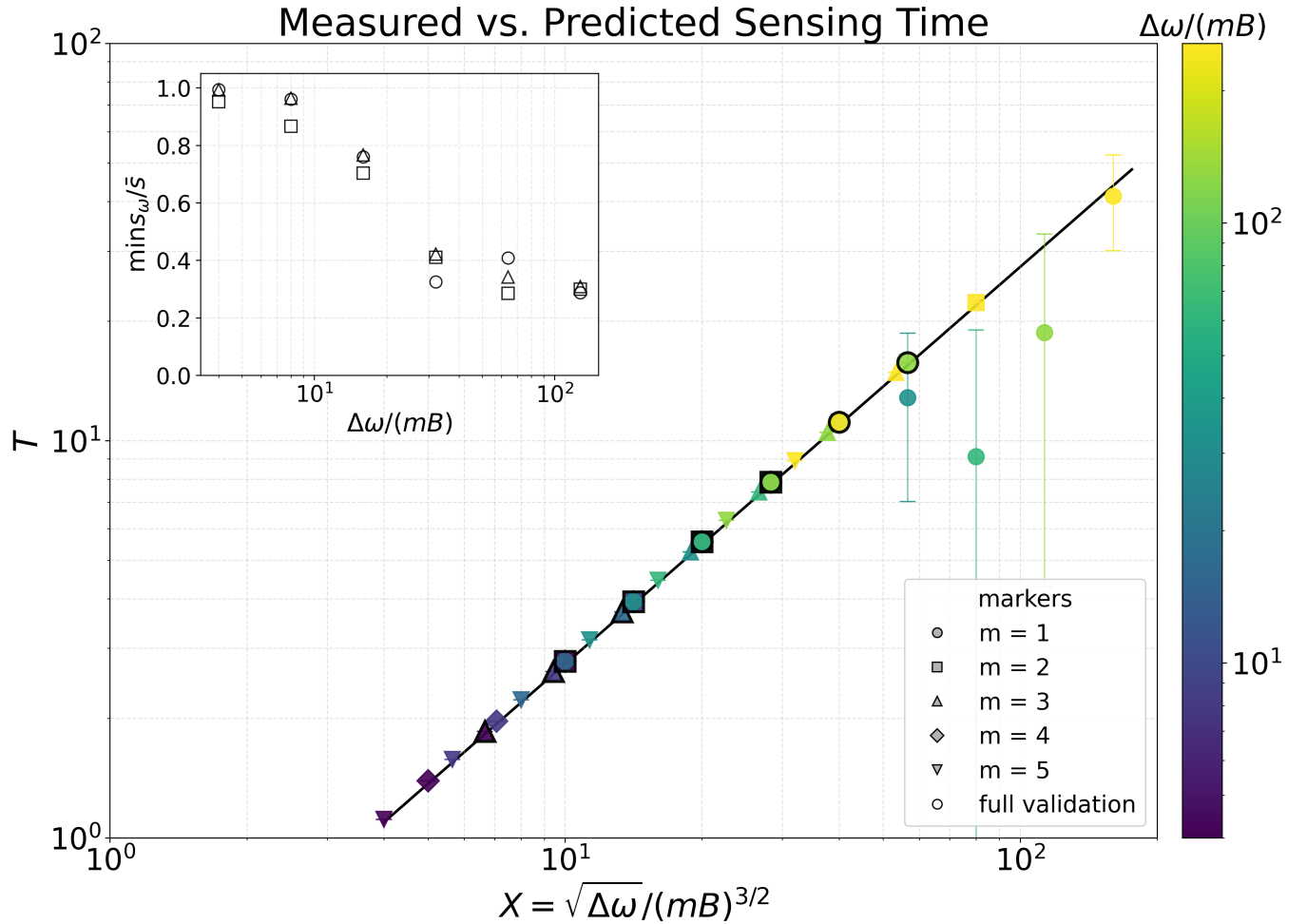


FIG. 2: Simulated stopping time T for the all-analog broadband protocol versus the predicted scale $X = \sqrt{|\Delta\omega|/(mB_{\min})^{3/2}}$ [Eq. (14)]. For each $(m, B_{\min}, \Delta\omega)$ we draw $\omega \sim \text{Unif}(\Delta\omega)$ and report the mean and standard deviation of the smallest T for which a fixed GHZ-diagonal population statistic exceeds a preset L_1 threshold (see End matter for more details). Time evolution uses a three-harmonic Floquet truncation; filled markers use a fast GHZ evaluation, while open markers show brute-force tensor-state validation at small m . We take $\omega_{\min} = 100$ MHz and $|\Delta\omega| \gg mB_{\min}$. The black line is unit slope to guide the eye. Inset: minimum normalized witness density $\min_{\omega} s_{\omega} / \bar{s}$ versus $\Delta\omega / B$ (equivalently, a flatness certificate against deep spectral holes, see the main text).

$\theta_{\omega}(B, T)^2$, its band integral $S(B, T) := \int_{\Delta\omega} d\omega s_{\omega}(B, T)$ and its average $\bar{s}(B, T) := S(B, T) / |\Delta\omega|$. We say the response is ε_T -flat if

$$\sup_{\omega \in \Delta\omega} \left| \frac{s_{\omega}(B, T)}{\bar{s}(B, T)} - 1 \right| \leq \varepsilon_T, \quad 0 \leq \varepsilon_T < 1. \quad (15)$$

Then for all $\omega \in \Delta\omega$,

$$\frac{|\Delta\omega|}{1 + \varepsilon_T} s_{\omega}(B, T) \leq S(B, T) \leq \frac{|\Delta\omega|}{1 - \varepsilon_T} s_{\omega}(B, T). \quad (16)$$

In particular, once ε_T is certified, a single observation of $s_{\omega^*}(B, T)$ determines $S(B, T)$ (and hence $K^{\text{FD}}(B, T) = \frac{4}{B^2} S(B, T)$) up to a constant factor.

All-analog broadband protocol To approach the lower bound in Eq. (14) without an incoherent scan over $\Delta\omega$, we replace external frequency scanning by internal band engineering by designing a static control Hamiltonian whose spectrum contains a dense set of transition frequencies spanning the entire search band, so that a single fixed experiment is simultaneously near-resonant with whichever tone frequency $\omega^* \in \Delta\omega$ happens to be present. The relevant spectral resolution is set by the collective (GHZ-enhanced) Rabi linewidth. For a driven two-level transition with effective coupling $\sim mB$ and detuning δ , the response is suppressed by a Lorentzian envelope $\eta(\delta) \sim (mB)^2 / ((mB)^2 + \delta^2)$ [32]. Thus frequencies separated by $\lesssim mB_{\min}$ are not meaningfully distin-

guishable in a worst-case broadband instance at amplitude B_{\min} . It is therefore natural to coarse-grain the band into

$$N \equiv \Theta\left(\frac{|\Delta\omega|}{mB_{\min}}\right) \equiv \Theta(r) \quad (17)$$

frequency “buckets” of width $\sim mB_{\min}$ (Fig. 1b).

The design objective is then to ensure that for every bucket there exists at least one active transition of the control Hamiltonian whose gap falls in that bucket. If this holds, then for any $\omega^* \in \Delta\omega$ the detuning to the nearest active gap obeys $|\delta| \lesssim mB_{\min}$, so $\eta(\delta) = \Theta(1)$ and the detection probability can be made uniform across the band up to constant factors.

We realize the above active-gap tiling using a finite Su-Schrieffer-Heeger (SSH) chain [33, 34]. Take a single register of dimension $d = \Theta(N)$ (equivalently $n = \log_2 d = O(\log r)$ qubits), and define an SSH Hamiltonian on $L = d/2$ unit cells,

$$G_{\text{SSH}} = \sum_{n=1}^L \left[t_1 c_{n,A}^\dagger c_{n,B} + t_2 c_{n+1,A}^\dagger c_{n,B} + \text{h.c.} \right], \quad (18)$$

(with periodic boundary conditions understood for notational simplicity). Up to finite-size corrections, the SSH spectrum consists of two bands so that we can engineer an interband gap $[\omega_{\min}, \omega_{\max}]$ that becomes dense as d increases. Intuitively, the SSH chain provides a minimal “resonant lattice” whose many internal gaps can be used as the bucket-tiling features required for broadband sensing. To ensure the control is approximately transverse to the signal (generalizing the Rabi example in [20]) we conjugate by an approximately Haar-random unitary U (approximable by nearly time-independent dynamics [35, 36]) and define $G_{\text{single}} := U G_{\text{SSH}} U^\dagger$ (see the End Matter for more details).

For the sensing state we use m identical noninteracting registers initialized to the generalized GHZ probe in the computational basis $|\psi_0\rangle = \frac{1}{\sqrt{d}} \sum_{i=0}^{d-1} |i\rangle^{\otimes m}$ with total control $G = \sum_{\ell=1}^m G_{\text{single}}^{(\ell)}$, evolve under the full Hamiltonian (Eq. (2)) for time T and then readout by projecting back onto the known $B = 0$ evolution. (Equivalently, we work in the interaction picture with respect to G , so that the no-signal state is exactly $|\psi_0\rangle$.) The two-outcome measurement $\{|\psi_0\rangle\langle\psi_0|, \mathbb{1} - |\psi_0\rangle\langle\psi_0|\}$ then yields $p_{\text{det}}(B, \omega, T) = 1 - |\langle\psi_0| U_G(T)^\dagger U(B, \omega; T) |\psi_0\rangle|^2 = 1 - |\langle\psi_0| U_I(B, \omega; T) |\psi_0\rangle|^2$, which is precisely the deviation probability relative to the $B = 0$ hypothesis.

Choosing the interrogation time to match the bound. The bucket picture also explains the time scaling. At amplitude B_{\min} the protocol’s sensitivity is distributed over $N = \Theta(r)$ resolvable spectral features, which dilutes the on-resonance response by a factor $\sim 1/\sqrt{N}$ at the level of amplitudes. The standard GHZ enhancement [16, 17] makes the relevant drive scale mB_{\min} , so near an active

bucket one obtains a resonant rotation angle of order $mB_{\min}T$ (up to $O(1)$ matrix-element factors), and hence a detection probability of the form $p_{\text{det}}(B_{\min}, \omega, T) = \Theta((mB_{\min}T)^2/N) \times \Theta(\eta(\delta))$, with $|\delta| \lesssim mB_{\min}$. Requiring constant detection probability uniformly over $\omega \in \Delta\omega$ therefore reduces to $(mB_{\min}T)^2/N = \Theta(1)$, i.e. $mB_{\min}T = \Theta(\sqrt{N}) = \Theta(\sqrt{r})$, which reproduces the lower-bound scaling in Eq. (14). For randomized tilings, rare large uncovered gaps can be suppressed by a mild oversampling $N = \Theta(r \log r)$ (equivalently $n = \log_2 r + \log_2 \log r + O(1)$), ensuring that the worst-case detuning remains $O(mB_{\min})$ (see End Matter).

The same lineshape intuition controls off-resonant contributions. If engineered active gaps are separated by steps of order mB_{\min} , then for a tone at frequency ω^* the nearest bucket contributes an $O(1)$ fraction of the resonant response, while other buckets at detunings $\delta \approx n mB_{\min}$ contribute only $\sum_{n \geq 1} \eta(n mB_{\min}) \sim \sum_{n \geq 1} 1/(1+n^2) = O(1)$, so multi-resonant crowding produces at most a constant-factor degradation. Thus the SSH-inspired resonant lattice implements a genuinely broadband, all-analog sensing strategy wherein a single coherent evolution time $T \sim \sqrt{|\Delta\omega|}/(mB_{\min})^{3/2}$, together with a simple GHZ-consistency readout suffices for detection across the full band.

Conclusion The SSH Hamiltonian gives a convenient and simple Hamiltonian for producing a distribution of energy differences across a band, however we note that similar constructions may be possible with superconducting TWPAs [37, 38] and integrated photonics which can be engineered to have flat frequency responses by realizing analogous passbands with coupled-resonator optical waveguides and photonic-crystal cavity arrays [39, 40], as well as ensemble light-matter interfaces which can emulate quasi-continuous spectra via controlled inhomogeneous broadening [41].

In total, we have shown that the Grover-like time scaling for broadband AC signal detection follows directly from an IQFI bandwidth ceiling and can be witnessed through a simple analog experiment. We have simulated this protocol and shown that it spreads sensitivity across an entire band by engineering many internal resonances (via a randomized SSH Hamiltonian) and probing them coherently with an m -register GHZ state, achieving the expected scaling in simulation. This suggests that the fundamental bound derived here, as well as in [20] and [15], is achievable without the need of quantum computation and provides a promising direction for its near-term implementation and experimental verification. Understanding robustness to decoherence and identifying minimal experimental implementations of the required multi-resonant controls are natural next steps.

Acknowledgements. This work was supported by this work was supported by NSERC-NSF alliance grant ALLRP-586858-2023 and an NSERC Discovery grant.

[1] C. L. Degen, F. Reinhard, and P. Cappellaro, Quantum sensing, *Reviews of Modern Physics* **89**, 035002 (2017).

[2] J. Bylander, S. Gustavsson, F. Yan, F. Yoshihara, K. Harrabi, G. Fitch, D. G. Cory, Y. Nakamura, J.-S. Tsai, and W. D. Oliver, Noise spectroscopy through dynamical decoupling with a superconducting flux qubit, *Nature Physics* **7**, 565 (2011).

[3] P. W. Graham, I. G. Irastorza, S. K. Lamoreaux, A. Lindner, and K. A. van Bibber, Experimental searches for the axion and axion-like particles, *Annual Review of Nuclear and Particle Science* **65**, 485 (2015).

[4] B. P. Abbott *et al.* (LIGO Scientific Collaboration and Virgo Collaboration), Observation of gravitational waves from a binary black hole merger, *Physical Review Letters* **116**, 061102 (2016).

[5] H.-Y. Huang, S. Choi, J. R. McClean, and J. Preskill, The vast world of quantum advantage, *arXiv preprint arXiv:2508.05720* (2025).

[6] R. Babbush, R. King, S. Boixo, W. Huggins, T. Khattar, G. H. Low, J. R. McClean, T. O'Brien, and N. C. Rubin, The grand challenge of quantum applications, *arXiv preprint arXiv:2511.09124* (2025).

[7] P.-J. Stas, Y.-C. Wei, M. Sirotin, Y. Huan, U. Yazlar, F. A. Arias, E. Knyazev, G. Baranes, B. Machielse, S. Grandi, *et al.*, Entanglement assisted non-local optical interferometry in a quantum network, *arXiv preprint arXiv:2509.09464* (2025).

[8] J. M. Brown and T. G. Walker, Perspective: Practical atom-based quantum sensors, *Physical Review A* **112**, 040102 (2025).

[9] S. A. Khan, S. Prabhu, L. G. Wright, and P. L. McMahon, Quantum computational sensing using quantum signal processing, quantum neural networks, and hamiltonian engineering, *arXiv preprint arXiv:2507.15845* (2025).

[10] J. Cotler, W. Gong, and I. Kannan, Noisy quantum learning theory, *arXiv preprint arXiv:2512.10929* (2025).

[11] J.-J. Feng, A. J. Brady, and Q. Zhuang, Physical-layer machine learning with multimode interferometric photon counting, *arXiv preprint arXiv:2506.12309* (2025).

[12] S. Liu, X. Wu, and M. Y. Niu, Optimal and robust in-situ quantum hamiltonian learning through parallelization, *arXiv preprint arXiv:2510.07818* (2025).

[13] D. Qian and J. Wang, Data-driven learnability transition of measurement-induced entanglement, *arXiv preprint arXiv:2512.01317* (2025).

[14] L. K. Grover, Quantum mechanics helps in searching for a needle in a haystack, *Physical Review Letters* **79**, 325 (1997).

[15] R. R. Allen, F. Machado, I. L. Chuang, H.-Y. Huang, and S. Choi, Quantum computing enhanced sensing, *arXiv preprint arXiv:2501.07625* (2025).

[16] M. J. Holland and K. Burnett, Interferometric detection of optical phase shifts at the heisenberg limit, *Physical review letters* **71**, 1355 (1993).

[17] J. J. Bollinger, W. M. Itano, D. J. Wineland, and D. J. Heinzen, Optimal frequency measurements with maximally correlated states, *Physical Review A* **54**, R4649 (1996).

[18] S. L. Braunstein and C. M. Caves, Statistical distance and the geometry of quantum states, *Physical Review Letters* **72**, 3439 (1994).

[19] A. M. Polloreno, *Characterizing Quantum Devices Using the Principles of Quantum Information*, Ph.D. thesis, University of Colorado at Boulder (2023).

[20] A. M. Polloreno, J. L. Beckey, J. Levin, A. Shlosberg, J. K. Thompson, M. Foss-Feig, D. Hayes, and G. Smith, Opportunities and limitations in broadband sensing, *Physical Review Applied* **19**, 014029 (2023).

[21] J. L. Beckey, *Theoretical Tools for Quantum Sensor Optimization and Entanglement Quantification*, Ph.D. thesis, University of Colorado at Boulder (2024).

[22] H. Shi and Q. Zhuang, Ultimate precision limit of noise sensing and dark matter search, *npj Quantum Information* **9**, 27 (2023).

[23] W. Hoeffding, Probability inequalities for sums of bounded random variables, *Journal of the American statistical association* **58**, 13 (1963).

[24] H. Chernoff, A measure of asymptotic efficiency for tests of a hypothesis based on the sum of observations, *The Annals of Mathematical Statistics* , 493 (1952).

[25] I. Bengtsson and K. Życzkowski, *Geometry of quantum states: an introduction to quantum entanglement* (Cambridge university press, 2017).

[26] A. Uhlmann, The “transition probability” in the state space of a^* -algebra, *Reports on Mathematical Physics* **9**, 273 (1976).

[27] C. A. Fuchs and J. Van De Graaf, Cryptographic distinguishability measures for quantum-mechanical states, *IEEE Transactions on Information Theory* **45**, 1216 (2002).

[28] D. Bures, An extension of kakutani's theorem on infinite product measures to the tensor product of semifinite w^* -algebras, *Transactions of the American Mathematical Society* **135**, 199 (1969).

[29] C. W. Helstrom, Minimum mean-squared error of estimates in quantum statistics, *Physics letters A* **25**, 101 (1967).

[30] D. Spehner, Bures geodesics and quantum metrology, *Quantum* **9**, 1715 (2025).

[31] K. Życzkowski and H.-J. Sommers, Average fidelity between random quantum states, *Physical Review A—Atomic, Molecular, and Optical Physics* **71**, 032313 (2005).

[32] M. O. Scully and M. S. Zubairy, *Quantum optics* (Cambridge university press, 1997).

[33] J. K. Asbóth, L. Oroszlány, and A. Pályi, *A Short Course on Topological Insulators: Band Structure and Edge States in One and Two Dimensions*, Lecture Notes in Physics, Vol. 919 (Springer, 2016).

[34] W. P. Su, J. R. Schrieffer, and A. J. Heeger, Solitons in polyacetylene, *Physical Review Letters* **42**, 1698 (1979).

[35] Y. Nakata, C. Hirche, M. Koashi, and A. Winter, Efficient unitary designs with nearly time-independent hamiltonian dynamics, *arXiv:1609.07021* (2017).

[36] N. LaRacuente and F. Leditzky, Approximate unitary k -designs from shallow, low-communication circuits, *arXiv preprint arXiv:2407.07876* (2024).

[37] C. Macklin, K. O'Brien, D. Hover, M. E. Schwartz, V. Bolkhovsky, X. Zhang, W. D. Oliver, and I. Siddiqi, A near-quantum-limited josephson traveling-wave parametric amplifier, *Science* **350**, 307 (2015).

[38] B. H. Eom, P. K. Day, H. G. LeDuc, and J. Zmuidzinas, A wideband, low-noise superconducting amplifier with high

dynamic range, *Nature Physics* **8**, 623 (2012).

[39] F. Morichetti, C. Ferrari, A. Canciamilla, and A. Melloni, The first decade of coupled resonator optical waveguides: bringing slow light to applications, *Laser & Photonics Reviews* **6**, 74 (2012).

[40] H. Takesue, N. Matsuda, E. Kuramochi, W. J. Munro, and M. Notomi, An on-chip coupled resonator optical waveguide single-photon buffer, *Nature Communications* **4**, 2725 (2013).

[41] N. Sangouard, C. Simon, M. Afzelius, and N. Gisin, Analysis of a quantum memory for photons based on controlled reversible inhomogeneous broadening, *Physical Review A* **75**, 032327 (2007).

[42] J. Watrous, *The Theory of Quantum Information* (Cambridge University Press, 2018).

[43] M. Ledoux, *The Concentration of Measure Phenomenon*, Mathematical Surveys and Monographs, Vol. 89 (American Mathematical Society, 2001).

[44] P. Hayden, Concentration of measure effects in quantum information, in *Quantum Information Science and Its Contributions to Mathematics*, Proceedings of Symposia in Applied Mathematics, Vol. 68 (American Mathematical Society, 2010) pp. 3–12.

[45] A. D. L. Mele, Introduction to haar measure tools in quantum information, *Quantum* **8**, 1340 (2024).

[46] C. Dankert, R. Cleve, J. Emerson, and E. Livine, Exact and approximate unitary 2-designs and their application to quantum randomizing, *Physical Review A* **80**, 012304 (2009).

Trotter Error

Equation (4) contains a “next-order” contribution scaling as $B^2 T^2 \delta t$ when a continuous-control protocol is approximated by piecewise-constant controls of step size δt . Here we give a short intuition for this dependence, following the Trotter-error analysis in Appendix IX D of Ref. [20]. For clarity, ignore the unknown phase and write (suppressing register indices)

$$H(t) = G(t) + B \cos(\omega t) Z_{\text{tot}}. \quad (19)$$

Approximating the time-ordered evolution by a first-order product formula with step size δt gives $N = T/\delta t$ segments, e.g.

$$U_0(T) \approx \prod_{k=0}^{N-1} \exp(-i G(t_k) \delta t) \exp(-i B \cos(\omega t_k) Z_{\text{tot}} \delta t), \quad t_k := k \delta t. \quad (20)$$

As shown in Ref. [20], bounding the IQFI of an N -operation (discrete) protocol gives a scaling $K = O(NT)$, and inserting $N = T/\delta t$ yields the leading contribution $O(T^2/\delta t)$. The key point is that the Trotterization error is controlled by the noncommutativity of the control and signal generators. For a step of size δt , the Baker–Campbell–Hausdorff expansion gives schematically

$$e^{-i(A+B)\delta t} = e^{-iA\delta t} e^{-iB\delta t} \exp\left(-\frac{\delta t^2}{2}[A, B] + O(\delta t^3)\right), \quad (21)$$

so with $A = G(t_k)$ and $B = B \cos(\omega t_k) Z_{\text{tot}}$ the leading remainder is generated by

$$-\frac{\delta t^2}{2} [G(t_k), B \cos(\omega t_k) Z_{\text{tot}}] = O\left(B \delta t^2 \|[G(t_k), Z_{\text{tot}}]\|\right). \quad (22)$$

Equivalently, one may view the product formula as simulating evolution under an effective Hamiltonian that includes an “error Hamiltonian”

$$H_{\text{err}}(t_k) \sim \frac{i \delta t}{2} [G(t_k), B \cos(\omega t_k) Z_{\text{tot}}], \quad \|H_{\text{err}}\| = O\left(B \delta t \|[G, Z_{\text{tot}}]\|\right), \quad (23)$$

since $-iH_{\text{err}}\delta t$ reproduces the $O(\delta t^2)$ exponent in (21). Because H_{err} is proportional to B , it perturbs the B -dependent generator of motion. The QFI (and hence IQFI) is quadratic in the state derivative $\partial_B |\psi\rangle$ (equivalently, quadratic in the generator for B), so a B -dependent perturbation of typical size $\|H_{\text{err}}\| \sim B\delta t$ contributes at second order:

$$J_{\text{err}}(B|\omega, T) \sim (\|H_{\text{err}}\| T)^2 = O\left(B^2 T^2 \delta t^2 \|[G, Z_{\text{tot}}]\|^2\right), \quad (24)$$

up to protocol-dependent $O(1)$ factors (e.g. commutator norms, time ordering).

The IQFI integrates $J(B|\omega, T)$ over ω . For a piecewise-constant discretization, each length- δt time bin has a Fourier width of order $1/\delta t$ (the Fourier transform of a time-domain rectangle is a sinc of width $\sim 1/\delta t$). Thus the discretization error in (24) is spread over an effective bandwidth $\Delta\omega_{\text{eff}} \sim 1/\delta t$, giving

$$K_{\text{err}}(B, T; \delta t) = \int d\omega J_{\text{err}}(B|\omega, T) \sim \Delta\omega_{\text{eff}} \times J_{\text{err}} = O\left(B^2 T^2 \delta t\right), \quad (25)$$

again up to protocol-dependent constants (absorbed into C_2 in Eq. (4)). This is the heuristic content of the T -independent coefficient $\alpha(\|G\|, B, \delta t)$ appearing in the continuous-protocol bound derived via Trotterization in Ref. [20]. Combining the discrete-protocol ceiling ($\propto T^2/\delta t$) with the Trotter-error contribution ($\propto B^2 T^2 \delta t$) yields precisely the structure of Eq. (4). Intuitively, making δt smaller increases the “available operations” $N = T/\delta t$ (boosting the first term), but decreases the noncommutativity-induced discretization error (suppressing the second term).

Approximate transversality under random conjugation

Let $d = 2^n$ and take $D = \sum_{k=1}^n Z_k$ on the n -qubit register. Let $\{|\psi_i\rangle\}_{i=1}^d$ be eigenvectors of $G_{\text{single}} = U G_{\text{SSH}} U^\dagger$. Then for $X_i = \langle\psi_i|D|\psi_i\rangle$,

$$\mathbb{E} X_i = 0, \quad \text{Var}(X_i) = \frac{n}{d+1}, \quad (26)$$

so a typical diagonal magnitude is $\Theta(\sqrt{n} 2^{-n/2})$. Moreover, by concentration of measure (Lévy's lemma) there exists a universal $c > 0$ such that for all $t > 0$, $\Pr(|X_i| \geq t) \leq 2 \exp\left(-c \frac{dt^2}{n^2}\right)$, using that $|\psi\rangle \mapsto \langle\psi| D |\psi\rangle$ is $2\|D\|_{\text{op}} = 2n$ -Lipschitz [42–46].

Numerical simulation and fast GHZ-population evaluation

This section describes the numerical procedure used to produce Fig. 2. We simulate the unitary dynamics generated by Eq. (2) with a static control $G = \sum_{\ell=1}^m G_{\text{single}}^{(\ell)}$ and a single-tone drive $B \cos(\omega t + \varphi) Z_{\text{tot}}$. Throughout we set $\varphi = 0$ without loss of generality (it is equivalent to a shift of the time origin for a time-independent G). All numerics assume coherent evolution (no decoherence) and ideal projective readout.

Parameterization, sampling, and stopping-time rule

We use the ratio $r := \frac{|\Delta\omega|}{mB_{\min}}$, and for each data point choose $|\Delta\omega| = r m B_{\min}$ and fix a high-frequency lower edge $\omega_{\min} = 100$ MHz, so that $\omega \in [\omega_{\min}, \omega_{\min} + |\Delta\omega|]$. Each plotted point in Fig. 2 aggregates multiple independent sensing instances: we draw ω uniformly from the band and also redraw the randomized control instance (random seed) so the error bars reflect both frequency variation and instance-to-instance variability. Concretely, for each fixed $(m, B_{\min}, |\Delta\omega|)$ we generate N_{samp} independent samples (ω, seed) and report the mean and standard deviation of the resulting stopping times. The reported sensing time is the first time at which a fixed detection statistic crosses a preset threshold.

Single-register control instance: SSH spectrum + randomized eigenbasis

To implement the “internal band engineering” discussed in the main text, each register is assigned a finite-dimensional Hilbert space of size $d = 2^n$ with $n = O(\log r)$ (in practice, we take d to be the nearest power of two to r , so that $d = \Theta(r)$). We build an SSH Hamiltonian on $L = d/2$ unit cells (periodic boundary conditions in the numerics),

$$G_{\text{SSH}} = \sum_{n=1}^L \left[t_1 c_{n,A}^\dagger c_{n,B} + t_2 c_{n+1,A}^\dagger c_{n,B} + \text{h.c.} \right], \quad (27)$$

with hopping amplitudes chosen so that the two SSH bands lie approximately at $\pm[A, B]$, where

$$A = \omega_{\min}/2, \quad B = (\omega_{\min} + |\Delta\omega|)/2, \quad t_1 = \frac{1}{2}(A + B), \quad t_2 = \frac{1}{2}(B - A). \quad (28)$$

Single-register time evolution via a three-harmonic Floquet truncation

For a fixed ω and effective drive amplitude B_{eff} , the single-register Hamiltonian

$$H_{\text{single}}(t) = G_{\text{single}} + B_{\text{eff}} \cos(\omega t) Z_{\text{single}} \quad (29)$$

is simulated using a three-harmonic Floquet truncation (Fourier modes $k \in \{-1, 0, +1\}$). In the Floquet basis, the truncated Floquet matrix is the $(3d) \times (3d)$ block matrix

$$F(\omega, B_{\text{eff}}) = \begin{pmatrix} G_{\text{single}} + \omega \mathbb{1} & \frac{B_{\text{eff}}}{2} Z_{\text{single}} & 0 \\ \frac{B_{\text{eff}}}{2} Z_{\text{single}} & G_{\text{single}} & \frac{B_{\text{eff}}}{2} Z_{\text{single}} \\ 0 & \frac{B_{\text{eff}}}{2} Z_{\text{single}} & G_{\text{single}} - \omega \mathbb{1} \end{pmatrix}. \quad (30)$$

We diagonalize $F = V \Lambda V^\dagger$ once per sample (ω, seed) . To obtain the physical single-register propagator $U_{\text{phys}}(t)$ at each time t on the ladder, we evolve the Floquet “initial condition” supported on the $k = 0$ sector (equivalently, evolve all d computational basis vectors at once by using $[0; \mathbb{1}; 0]$ as a block right-hand-side), and reconstruct

$$U_{\text{phys}}(t) = e^{+i\omega t} Y_{+1}(t) + Y_0(t) + e^{-i\omega t} Y_{-1}(t), \quad (31)$$

where $Y_{\pm 1,0}(t)$ are the $d \times d$ blocks of the evolved Floquet solution in the $k = \pm 1, 0$ sectors. Finally, we convert to the interaction picture with respect to G_{single} , $U_I(t) = e^{+iG_{\text{single}}t} U_{\text{phys}}(t)$.